ACS OMEGA

http://pubs.acs.org/journal/acsodf

Article

# Microwave Irradiation-Assisted Reversible Addition−Fragmentation Chain Transfer Polymerization-Induced Self-Assembly of pH-Responsive Diblock Copolymer Nanoparticles

Svetlana Lukáš Petrova,* Vladimir Sincari,* Rafał Konefał, Ewa Pavlova, Martin Hrubý, Václav Pokorný, and Eliézer Jäger

Cite This: *ACS Omega* 2022, 7, 42711−42722

Read Online

ACCESS | Metrics & More | Article Recommendations | Supporting Information

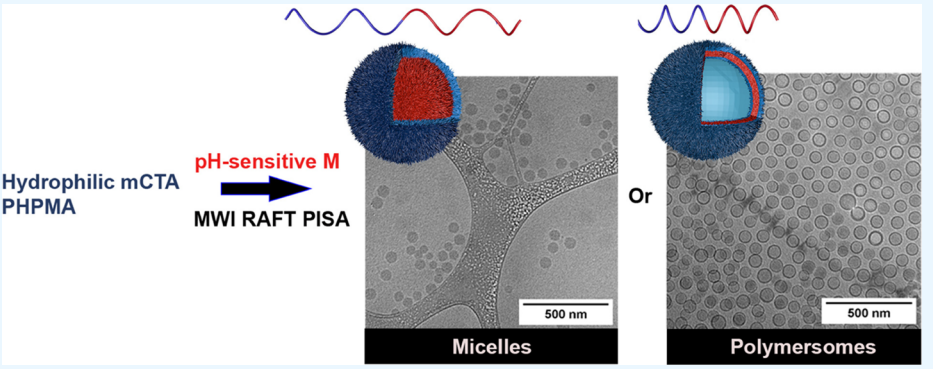


**ABSTRACT:** Herein, we present a versatile platform for the synthesis of pH-responsive poly([*N*-(2-hydroxypropyl)]-methacrylamide)-*b*-poly[2-(diisopropylamino)ethyl methacrylate] diblock copolymer (PHPMA-*b*-PDPA) nanoparticles (NPs) obtained via microwave-assisted reversible addition−fragmentation chain transfer polymerization-induced self-assembly (MWI-PISA). The *N*-(2-hydroxypropyl) methacrylamide (HPMA) monomer was first polymerized to obtain a macrochain transfer agent with polymerization degrees (DPs) of 23 and 51. Subsequently, using mCTA and 2-(diisopropylamino)ethyl methacrylate (DPA) as monomers, we successfully conducted MWI-PISA emulsion polymerization in aqueous solution with a solid content of 10 wt %. The NPs were obtained with high monomer conversion and polymerization rates. The resulting diblock copolymer NPs were analyzed by dynamic light scattering (DLS) and cryogenic-transmission electron microscopy (cryo-TEM). cryo-TEM studies reveal the presence of only NPs with spherical morphology such as micelles and polymer vesicles known as polymersomes. Under the selected conditions, we were able to fine-tune the morphology from micelles to polymersomes, which may attract considerable attention in the drug-delivery field. The capability for drug encapsulation using the obtained in situ pH-responsive NPs, the polymersomes based on $PHPMA_{23}$-*b*-$PDPA_{100}$, and the micelles based on $PHPMA_{51}$-*b*-$PDPA_{100}$ was demonstrated using the hydrophobic agent and fluorescent dye as Nile red (NR). In addition, the NP disassembly in slightly acidic environments enables fast NR release.

## INTRODUCTION

Amphiphilic block copolymers self-assembled into highly organized nanoscale structures in an aqueous milieu have attracted considerable attention for decades.[1−4] Such nanoparticles (NPs) have been widely investigated both experimentally and theoretically owing to many potential applications. From a thermodynamic point of view, favored structures of various morphologies in solution strongly depend on changes in the solvent selectivity or the insoluble-to-soluble block length ratio.[3] Furthermore, by thoroughly changing different variables, including the monomer concentration, degree of polymerization, and solvent composition, a diversity of morphologies, such as spheres, worms, vesicles, lamellae, or sunflowers, can be obtained. However, these NPs are prepared by the self-assembly of block copolymers via a post-polymerization process, a strategy that is hindered due to very low concentrations of polymers (∼1 wt %).[5−8]

Over the past decade, increasing attention has been given to the development and use of polymerization-induced self-assembly (PISA) as an efficient technique for the preparation of block copolymer nanoassemblies.[9−11] In contrast to conventional assembly processes, PISA allows the in situ

Received: June 28, 2022
Accepted: October 18, 2022
Published: November 17, 2022

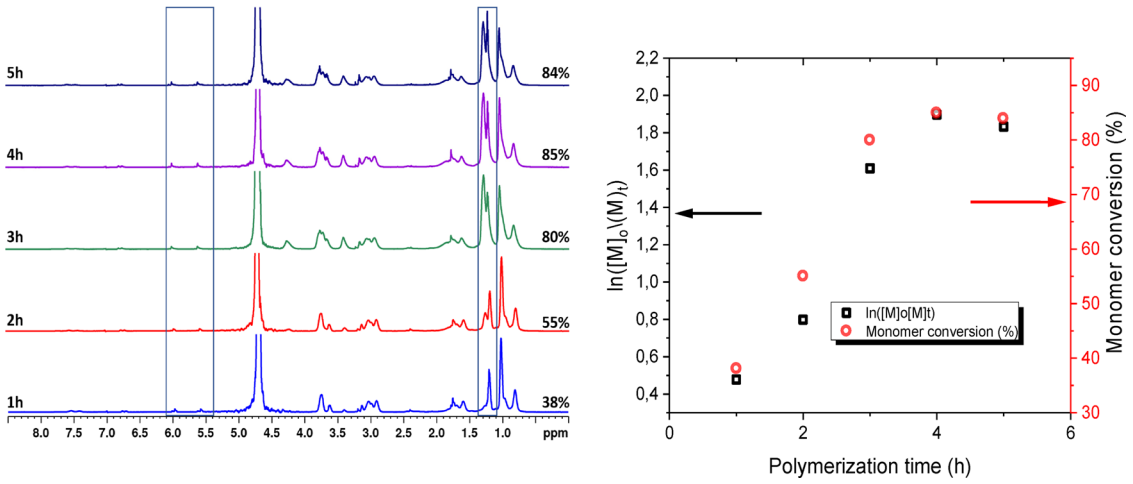


**Figure 1.** $^1$H NMR spectra recorded in $D_2O$ + 10 $\mu$L DCl (left) and conversion vs time course (red circles) corresponding to the semi-logarithmic plot (black squares) during the MWI-PISA polymerization of $PHPMA_{23}$-*b*-$PDPA_{50}$ (right).

production of NPs in a one-pot approach at high solid concentrations (up to 50 wt %),[12−14] without recourse to any additional purification steps with tunable size, morphology, and functionality.[15−17] The process consists of a soluble polymer in an appropriate solvent becoming insoluble after chain extension by the polymerization of a second monomer. This contributes to the spontaneous self-assembly of sterically stabilized NPs, where the diverse size and morphology strongly depend on the relative volume ratio of each block and on the solid content.[18,19]

Various types of controlled/living radical polymerization techniques have been utilized to conduct the PISA method.[20−22] Reversible addition−fragmentation chain transfer (RAFT) has proven to be the most successful and powerful platform for PISA syntheses.[23−25] Furthermore, using either emulsion or dispersion polymerization, the RAFT-mediated PISA technique can be accomplished in a wide range of monomers and various reaction media such as organic polar solvents (e.g., lower alcohols such as methanol or ethanol),[26,27] organic nonpolar solvents (typically *n*-alkanes),[28−30] and especially water.

Extensive studies have been initially performed on RAFT aqueous emulsion polymerization using water-immiscible monomers such as *n*-butyl acrylate, methyl methacrylate, or styrene.[31−35] Later, however, it was found that this synthetic technique in many cases leads only to the formation of spherical NPs, rather than the full range of copolymer morphologies.[36−38] However, despite the limitations, recently, Armes and co-workers[39] have successfully synthesized diblock copolymer spheres, worms, and vesicles *via* RAFT aqueous emulsion polymerization based on hydroxybutyl methacrylate.

The RAFT dispersion polymerization (RAFTDP) successfully produces particles of variable and complex morphology, including spheres, worms, and vesicles[26,40−43] displaying uniform physico-chemical properties. Detailed studies on RAFTDP-PISA, especially in aqueous media, have been performed[44−46] using various macro-RAFT agents including poly(glycerol monomethacrylate),[47] poly(ethylene glycol),[48] poly(2-(dimethylamino) ethyl methacrylate),[49] poly(amino acid methacrylate),[50] and others.

We aim to explore the microwave irradiation-PISA (MWI-PISA) approach for the in situ preparation of nanomaterials assembled from pH-sensitive poly([*N*-(2-hydroxypropyl)]-methacrylamide)-*b*-poly[2-(diisopropylamino)ethyl methacrylate] block copolymers ($PHPMA_m$-*b*-$PDPA_n$) (Figure 1). The obtained assemblies may find applications in biomedical fields. It is well known that PHPMA has been extensively investigated as a hydrophilic component because it is a water-soluble, nontoxic, nonimmunogenic, and biocompatible polymer.[46−48] PHPMA-based polymers have been widely used in drug- and gene-delivery vehicles or as NPs to carry drugs, for surface modification of NPs, polymer−biomolecule conjugation, and bioimaging.[51−54] The tertiary amine group of the DPA monomer allows to control the extent of positive charge via protonation that is dictated by the pH changes, for example, via the addition of HCl to attain pH values below its $pK_a$ ∼ 6.2−6.3, where DPA becomes hydrophilic.[55,56] This property renders pH-sensitive NPs based on PDPA attractive for tumor-targeting drug delivery with the capability of encapsulating guest drug molecules.[51,55]

It should be noted that there is only one reported microwave irradiation evaluation on the synthesis of soft matter nano-objects via PISA-RAFTDP using methanol as a solvent and poly[oligo(ethylene glycol) methyl ether methacrylate] as a macroinitiator.[57] In addition, this study examines in detail the comparison of microwave-assisted synthesis with conventional heating one in RAFTDP-PISA formulations, where it was proved that the MWI method could be successfully applied to PISA nano-objects.

Indeed, the microwave irradiation (MWI) has emerged as a powerful technique offering simple, clean, fast, efficient, and economical method for the synthesis of a large number of biologically active molecules for organic synthesis, inorganic synthesis, material science, polymer chemistry, and other disciplines. The preparation of block copolymers *via* MWI using different polymerization techniques is well-studied and increasingly used and is rarely reported for PISA. Recently, in our previously published work, we clearly demonstrated the MWI technique as a rapid and useful tool for the synthesis of PHPMA-mCTA and its copolymers.[58]

To the best of our knowledge, this is the first very straightforward strategy to obtain pH-responsive highly monodisperse nanoparticles implemented by RAFT aqueous polymerization of DPA using PHPMA-mCTA with calibrated degrees of polymerization (DP) of 23 and 51, respectively, via the combination of the MWI method with the PISA technique.


https://doi.org/10.1021/acsomega.2c04036
ACS Omega 2022, 7, 42711−42722

Such an efficient, aqueous MWI-PISA method to produce uniform spherical NPs with controlled morphologies at solid contents up to 10% w/w represents important progress in the nano-field. Furthermore, to demonstrate the potential application of such nanotechnology-based polymerization approach in cancer therapies, where a low local pH is commonly found, a lipophilic stain (such as Nile red) was used as a drug model. The resulting nano-objects and structure were characterized in detail by cryogenic-transmission electron microscopy (cryo-TEM), small-angle X-ray scattering (SAXS), dynamic light scattering (DLS), and static light scattering (SLS) techniques. Besides, the obtaining NPs are below the renal threshold while their size fits well the requirements for drug-delivery purposes.

## EXPERIMENTAL SECTION

**Materials.** The monomer *N*-(2-hydroxypropyl)-methacrylamide (HPMA) (Scheme S1 and Figure S1) was synthesized according to a previous study,[59] and 4-cyano-4-(((ethylthio)carbonothioyl)thio)pentanoic acid was synthesized as reported earlier[60] (Scheme S2 and Figure S2).

Chemicals: 1-amino-2-propanol (93%), methacryloyl chloride (≥97.0%, distilled under an argon atmosphere), sodium hydride (NaH, 60% dispersion in mineral oil), ethanethiol (EtSH, 97%), carbon disulfide ($CS_2$, anhydrous, ≥99%), triethylamine ($Et_3N$, ≥99.5%), 4,4′-azobis(4-cyanovaleric acid) (V-501, ≥98%), 2-(diisopropylamino)ethyl methacrylate (97%, distilled under an argon atmosphere), and Nile red (NR) BioReagent, ≥97.0% (HPLC) were purchased from Sigma-Aldrich Ltd. (Czech Republic). Solvents (all purchased from Sigma-Aldrich Ltd. (Czech Republic): dichloromethane ($CH_2Cl_2$, anhydrous ≥99.8%) was dried by refluxing over a benzophenone-sodium complex and distilled under an argon atmosphere. Other solvents including diethyl ether ($Et_2O$, ≥99.7%), dimethyl sulfoxide (DMSO, ≥99.5%), and *tert*-butanol (*tert*-BuOH, ≥99.5%) were used as received.

**Synthesis of PHPMA-mCTA via MWI (Scheme 1, (1)).** The RAFT polymerization of HPMA was performed in the Biotage Initator + Microwave System with Robot Sixty using a Biotage high-precision MW glass vial (10−20 mL) and conducted with a laboratory MW reactor. The MW instrument was set to a normal absorption level with a prestirring step of 60 s. A typical procedure for the polymerization was as follows: first, a monomer HPMA (1.0 g, $1.25 \times 10^{-4}$ mol) was dissolved in *tert*-BuOH (5 mL) and placed in vials equipped with a magnetic stirring bar. Then, CTA (58 mg in the case of DP 21 and 32.9 mg in the case of DP 51) and initiator V-501 (40 mg in the case of DP 23 and 17.5 mg in the case of DP 51) ([CTA]/[I] 1/0.2) (CTA/I molar ratio = 5 based on the reaction conditions established in our previous study toward obtaining macrochain transfer agents with the lowest dispersity)[58] were dissolved in 50 μL of dimethylsulfoxide (DMSO) and then transferred to the monomer solution. The vial was sealed and deoxygenated for 30 min using argon purging. Afterward, the vial was placed in the cavity of the MW instrument, and the temperature was set to 75 °C, with a reaction time of 3 h. Then, the polymerization was stopped by ceasing MWI, removing the vial from the instrument and rapidly quenching in liquid nitrogen and analyzed by $^1$H NMR spectroscopy. The remaining fraction of the sample solution was precipitated into cold acetone or an acetone/ether mixture 3/1 (v/v) for molecular weight analysis.

**PISA Synthesis of PHPMA$_m$-*b*-PDPA$_n$ NPs via MWI (Scheme 1, (2)).** MWI-PISA RAFT polymerization at 10% w/w solids in aqueous solution was carried out as follows: in a vial (2 mL) equipped with a magnetic stirrer, PHPMA-mCTA (20 mg) was dissolved in water. Afterward, water-immiscible 2-(diisopropylamino)ethyl methacrylate (DPA) and the initiator V-501 (0.5 mol·L$^{-1}$, related to PHPMA-mCTA, where 0.18 mg was used for DP 23 and 0.19 mg for DP 51)) ([CTA]/[I] 1/0.5) were added to the aqueous solution. In case of PHPMA$_{23}$-mCTA, the amount of the DPA monomer was (at DP 50 22 μL, DP 75 33 μL, and DP 100 44 μL). In case of PHPMA$_{51}$-mCTA, the amount of the DPA monomer was (at DP 50 23.22 μL, DP 75 34 μL, and DP 100 45 μL). The glass vial was sealed and then purged with argon for 30 min. Next, the reaction vial was placed in the cavity of the MW instrument, and the temperature was programmed to 75 °C. After 5 h, the polymerization was stopped with a quenching step using liquid nitrogen. The monomer conversions in case of PHPMA$_{23}$-*b*-PDPA$_{50}$ and the structure of block copolymers from in situ obtained NPs were confirmed by $^1$H NMR spectroscopy. Furthermore, the resulting NPs were analyzed by cryo-TEM and DLS, as well.

**PISA Synthesis of PHPMA-*b*-PDPA$_{NR}$ NPs via MWI.** NR, a polarity-sensitive hydrophobic dye, was selected as the model drug and it was encapsulated via MWI-PISA RAFT polymerization at 10% w/w solids in water. The NPs were synthesized targeting DP 100 of the hydrophobic core. NR was dissolved in the monomer (DPA) and PHPMA-mCTAs with DP 23 and 51 chosen. In a typical experiment, PHPMA-mCTA (20 mg) was dissolved in deionized water under stirring for 10 min in the MW vial, and then, the initiator V-501 (0.22 mg) was added. After that, the hydrophobic monomer DPA (51 μL) with NR (500 μg) was added. The vial was sealed and degassed for 30 min under argon flow being subsequently immersed in the cavity of the MW instrument. The temperature was set to 75 °C, with a reaction time of 5 h. The resulting PHPMA-*b*-PDPA$_{NR}$ NPs were purified using the G50 column in PBS (pH 7.4) to remove unloaded NR and then analyzed by DLS, high-performance liquid chromatography (HPLC), and cryo-TEM.

**NR Encapsulation Efficiency and Release.** The NR content and NR release from the NPs was measured by HPLC (Ultimate 3000 HPLC, Thermo Fisher Scientific) using a reverse-phase column Chromolith Performance RP-18e (100 × 4.6 mm, eluent water−acetonitrile with acetonitrile gradient 0−100 vol %, flow rate = 2.0 mL·min$^{-1}$). The analytical curve with a linear response in the range 0.001−0.1 mg·mL$^{-1}$ was recorded using a fluorescence detector and used to determine the NR-loaded content. The drug-loading content (LC) and the drug-loading efficiency (LE) were calculated by using the following equations:

$$\mathrm{LC}(\%) = \frac{\text{drug amount in nanoparticles}}{\text{mass of nanoparticles}} \times 100 \quad (1)$$

$$\mathrm{LE}\ (\%) = \frac{\text{drug amount in nanoparticles}}{\text{drug amount used for encapsulation}} \times 100 \quad (2)$$

The LC and LE of NR were determined by HPLC. The NR quantification was determined according to the calibration curve with a linear response in the range 0.001−0.5 mg·mL$^{-1}$. The values were calculated using the standard eqs 1 and 2. The NR cumulative release was evaluated using the dialysis method in PBS buffer at pH 7.4 and in acetate buffer at pH 4. A



https://doi.org/10.1021/acsomega.2c04036
ACS Omega 2022, 7, 42711−42722

**Scheme 1. General Outline for the PISA Synthesis of PHPMA-*b*-PDPA Block Copolymers, and Their Associated Nanoparticles under MWI Conditions**

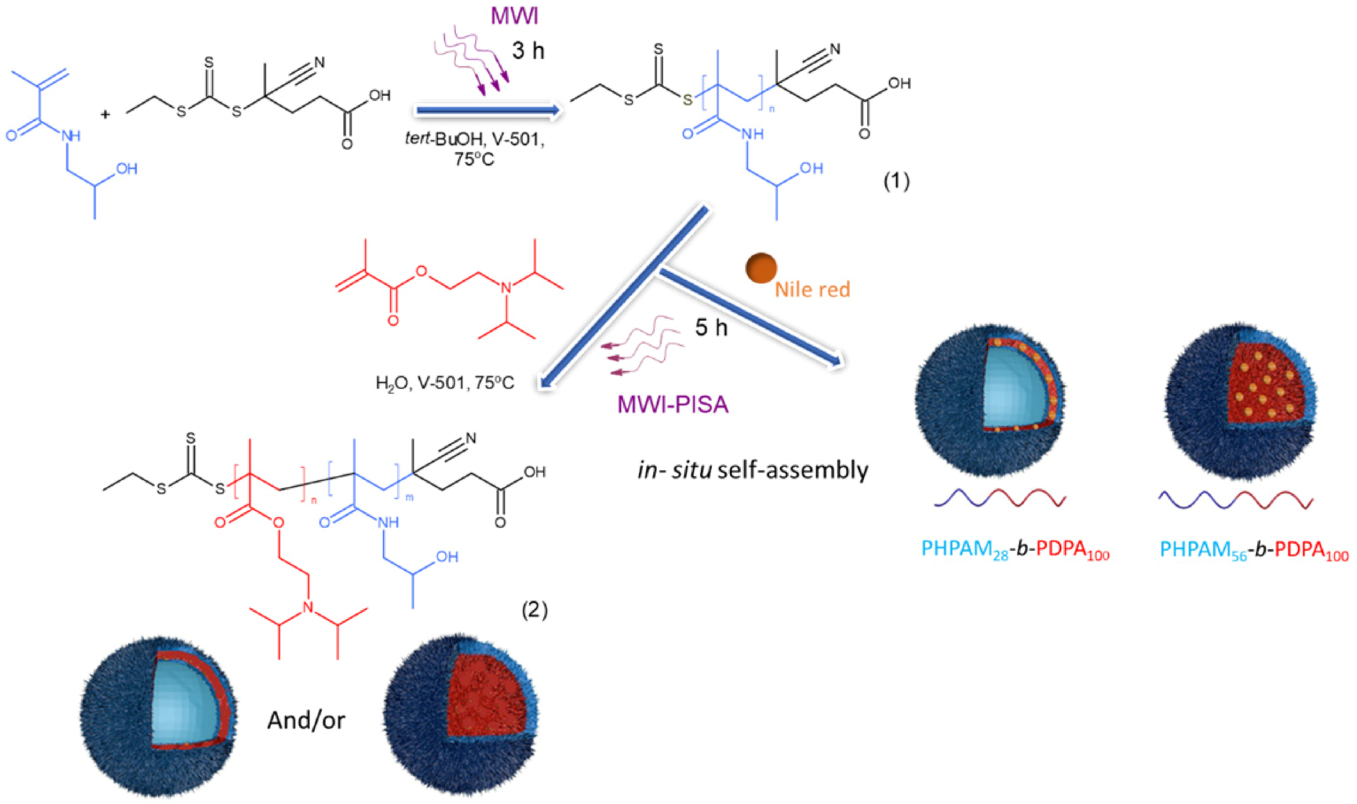


**Table 1. Macromolecular Characteristics of the PHPMA-mCTAs**

| entry | sample | DP | $M_n$,[a] (theor.) ($moL^{-1}$) | $M_n$,[b] (SEC) (g $moL^{-1}$) | $Đ$,[c] (SEC) |
|---|---|---|---|---|---|
| 1 | PHPMA-mCTA | 23 | 3200 | 3890 | 1.15 |
| 2 | PHPMA-mCTA | 51 | 7400 | 7650 | 1.05 |

[a] $M_n = [M]_o/[I]_o \times$ conv. $\times M_{WHPMA} + M_{WCTA}$ (ESI, Figure S3). [b] $M_n$ value (Supplementary Materials, Figure S4). [c] $Đ$ value (Supplementary Materials, Figure S4).

preswollen cellulose dialysis membrane tube with MWCO 3.5−5 kDa (Spectra-Por Float-A-Lyzer G2) was filled with 2.0 mL of NR-loaded NPs at 5 mg·$mL^{-1}$. The membrane tube was then immersed into 3 L of the buffers at 37 °C under stirring (500 rpm). At predetermined times, 10 $\mu$L of the NR-loaded NPs was taken from the membrane tube and diluted into 90 $\mu$L of DMSO to determine the amount of remaining NR, as measured by HPLC.

## RESULTS AND DISCUSSION

To obtain higher-ordered morphologies, such as micelles or polymersomes, shorter macro-RAFT agents were used. Thus, well-defined PHPMA-mCTAs were successfully synthesized by RAFT *via* MWI using 4-cyano-4-(((ethylthio)carbonothioyl)-thio)pentanoic acid as CTA (Scheme 1, (1)). The polymerization was performed according to our previously reported literature protocol[58] using an MW reactor at 75 °C with 4,4′-azobis(4-cyanovaleric acid) (V-501) as the initiator.

The chemical structure, molecular weight, and dispersity of the obtained PHPMA-mCTAs were analyzed by $^1$H NMR spectroscopy and size exclusion chromatography (SEC) (see ESI, Figures S3 and S4). $^1$H NMR measurement confirmed the successful preparation of PHPMA-mCTA, as shown in Figure S3, ESI. The obtained PHPMA$_n$-mCTAs have a DP of 23 and 51, calculated from the monomer conversion (molecular weight of PHPMA-mCTA was not calculated by $^1$H NMR, because the signals assigned to the end group of the macroinitiator with a higher DP were not visible in the spectrum), and the macro-RAFT agents are denoted as PHPMA$_{23}$-mCTA and PHPMA$_{51}$-mCTA, respectively. SEC chromatograms of both PHPMA-mCTAs are indicated by the overlap of the SEC traces and demonstrated monomodal distribution (see Figure S4, in ESI). The macromolecular characteristics of the PHPMA-mCTAs are listed in Table 1.

To assess the efficiency of the MWI-PISA formulation of DPA in aqueous media, water-soluble PHPMA-mCTA was used (Scheme 1). DPA has poor solubility in water under neutral and basic conditions, which leads to the in situ formation and self-assembly of the PDPA block by emulsion polymerization. First, to determine the reaction time and monomer conversion during MWI-PISA polymerization, a kinetic study was conducted. The kinetics of reactions targeting a mean DP of 50 for the core-forming PDPA block (PHPMA$_{23}$-*b*-PDPA$_{50}$) at 10% w/w solids in water were monitored, see Figure 1. Therefore, at different time points, the polymerization was stopped by ceasing MWI, removing the vial from the instrument and rapidly quenching in liquid nitrogen.



https://doi.org/10.1021/acsomega.2c04036
ACS Omega 2022, 7, 42711−42722

Table 2. Summary of Final DPA Monomer Conversions, Intensity-Average DLS Particle Diameter, and Cryo-TEM Morphologies Obtained for $PHPMA_m$-b-$PDPA_n$, Diblock Copolymer Nanoparticles after 5 H MWI-PISA in Water

| n | target composition | $[M]_0/[CTA]_0/[I]_0$ | conv. (%)[a] | Mn ($^1$H NMR)[b] | $D_H$/nm, (PDI)[c] | morph.[d] | D/nm[e] | wt (%) PHPMA[f] |
|---|---|---|---|---|---|---|---|---|
| 1 | $PHPMA_{23}$-b-$PDPA_{50}$ | 50/1/0.5 | 85 | 13,100 | 60 (0.09) | M | 40 | 24 |
| 2 | $PHPMA_{23}$-b-$PDPA_{75}$ | 75/1/0.5 | 92 | 18,700 | 65 (0.185) | M + PSs | 50 | 17 |
| 3 | $PHPMA_{23}$-b-$PDPA_{100}$ | 100/1/0.5 | 80 | 21,000 | 123 (0.05) | PSs | 100 | 15 |
| 1 | $PHPMA_{51}$-b-$PDPA_{50}$ | 50/1/0.5 | 88 | 17,400 | 59 (0.094) | M | 30 | 42 |
| 2 | $PHPMA_{51}$-b-$PDPA_{75}$ | 75/1/0.5 | 87 | 21,900 | 165 (0.073) | M | 90−160 | 34 |
| 3 | $PHPMA_{51}$-b-$PDPA_{100}$ | 100/1/0.5 | 81 | 24,400 | 183 (0.11) | M | 130 | 30 |

[a]Conversion determined by $^1$H NMR spectroscopy. [b]$M_n$ determined by $^1$H NMR. [c]Hydrodynamic diameter and dispersity from DLS. [d]Nanoparticle morphology from cryo-TEM (M = micelles and PSs = polymersomes). [e]Particle diameter from cryo-TEM. [f]Weight fraction of PHPMA calculated based on $^1$H NMR.

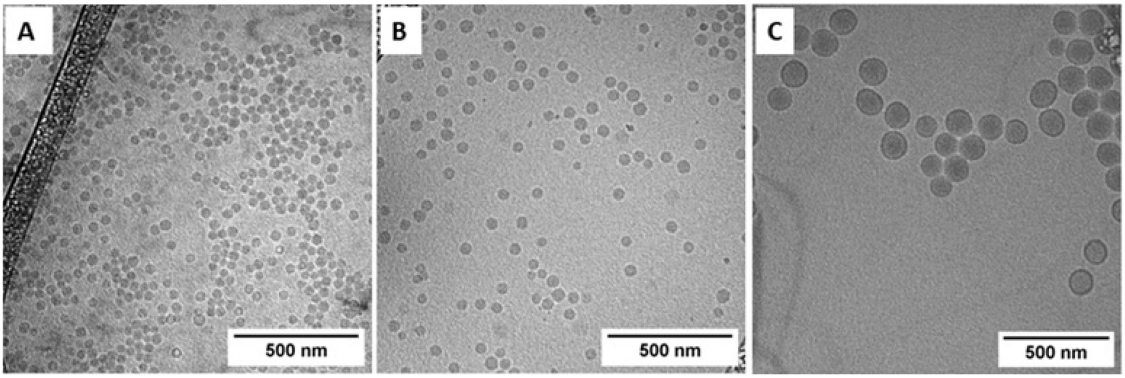


Figure 2. Cryo-TEM images of $PHPMA_{23}$-b-$PDPA_{50}$ (A), $PHPMA_{23}$-b-$PDPA_{70}$ (B), and $PHPMA_{23}$-b-$PDPA_{100}$ (C) nanoparticles formed in water at 10% w/w solids under MWI conditions.

An aliquot of the sample solution (20 μL) was immediately analyzed by $^1$H NMR spectroscopy (Figure 1 left).

The $^1$H NMR kinetic study was conducted to investigate the monomer conversion as well as the polymerization rate over time caused by partitioning of the unreacted monomer within the growing NPs. Figure 1, left, shows the kinetic data obtained for the synthesis of the $PHPMA_{23}$-b-$PDPA_{50}$ diblock copolymer via aqueous RAFT polymerization at 10% w/w solids, 75 °C and utilizing a CTA/initiator molar ratio of 2.0 (based in conditions stablished in our previous study toward obtaining the PHPMA-b-PDPA block with the highest conversion).[61] The monomer conversion was calculated by comparing the integrals of the remaining vinyl signals of DPA at 5.5 and 6.0 ppm with methylene signals $(CH_2)_4$ of the DPA monomer and polymer. It is well known that PDPA is insoluble in deuterated water, which implies the absence of an NMR signal for PDPA. Therefore, 10 μL of deuterated hydrochloric acid (DCl) was added to protonate insoluble PDPA, making its signals visible. As shown in Figure 1, left, a series of spectra recorded at various stages of MWI-PISA polymerization demonstrated visible signals of the DPA monomer at approximately 5.5 and 6.0 ppm up to a monomer conversion of ∼38% in the first hour. At higher conversions, these signals are still visible; however, they become weaker and disappear at higher conversions of ∼85% (4 h, Figure 1 left). According to a previous hypothesis, along PISA polymerization, unreacted monomers solvate the core-forming chains,[62] increasing the polymerization rate; however, we observed a plateau at the 4−5 h (Figure 1 left) time course of polymerization.

Examining the kinetic plots of $\ln([M]_o/[M]_t)$ (Figure 1 right), a clear increase in the rate of polymerization over time is observed. The plot was linear until the fourth hour from the beginning of PISA polymerization, after which a plateau was reached (Figure 1 right). After 4 h of polymerization, almost complete monomer conversion (∼85%) was achieved. These data showed that the MWI-PISA aqueous RAFT polymerization proceeded with reasonably good control, achieving high conversion (∼85%) within a short period of time (4 h). To ensure efficient RAFT control, the molar ratio between the macro-RAFT agent and PDPA $DP_n$ was varied ($n$ = 50, 75, and 100) at 10% w/w solids in all aqueous MWI-PISA formulations. It can be clearly seen that the increase in the targeted DP of PDPA leads to no significant increase in conversion, see Table 2. This occurs probably due to the "nanoprecipitation" nature of polymerization, where sufficiently long growing PDPA chain precipitates and forms the nanoparticle core, which significantly reduces its reactivity toward further polymerization.[62]

It is well described that targeting different DPs of the corresponding hydrophobic block influence the morphology of the obtained NPs. Hence, the morphology of the obtained PISA formulations in water was characterized by cryo-transmission electron microscopy (cryo-TEM), and the particle size was characterized by DLS. A small amount was diluted with water to approximately 1 $mg{\cdot}mL^{-1}$ (for cryo-TEM) and 0.1 $mg{\cdot}mL^{-1}$ (for DLS). According to the DLS data, with an increase in the DP of the DPA monomer, the mean particle diameter increased consistently with the theoretical expectation of the increase in the NP core size. The same trend was observed in the cryo-TEM measurements. In all cases, spherical NPs were obtained, with diameters generally in agreement with DLS; in addition, micelle-to-vesicle morphological transitions of the NPs can be observed in


https://doi.org/10.1021/acsomega.2c04036
ACS Omega 2022, 7, 42711−42722

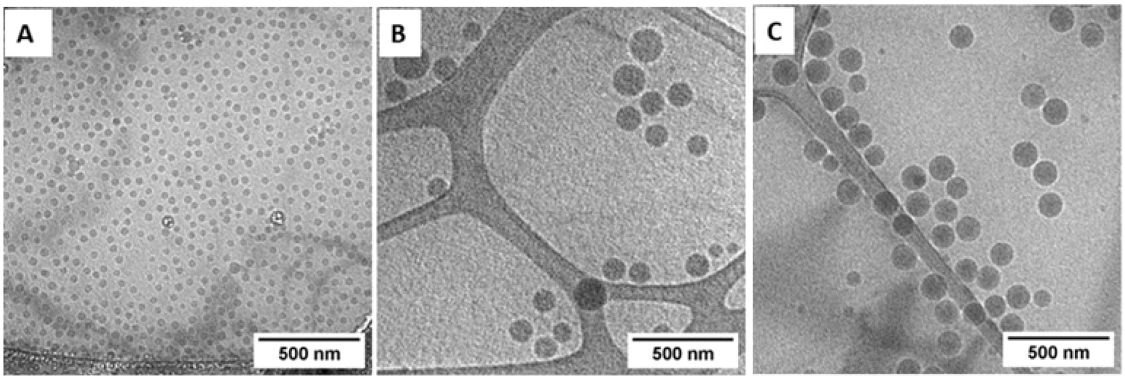


**Figure 3.** Cryo-TEM images of the $PHPMA_{51}$-*b*-$PDPA_{50}$ (A), $PHPMA_{51}$-*b*-$PDPA_{70}$ (B), and $PHPMA_{51}$-*b*-$PDPA_{100}$ (C) nanoparticles formed in water at 10% w/w solids under MWI conditions.

case with the use of relatively short PHPMA-mCTA (DP 23). The resultant cryo-TEM morphologies for all copolymer NPs are illustrated in Figures 2 and 3, respectively. The corresponding DLS particle size distributions are shown in Figures S5 and S7 (see the Supporting Information section). Physicochemical characteristics of NP formulations are listed in Table 2.

The TEM image of $PHPMA_{23}$-*b*-$PDPA_{50}$ (Figure 2A) demonstrates uniform and well-defined NPs with spherical shapes with a DLS-measured hydrodynamic diameter of 60 nm and polydispersity = 0.09 (Figure S5, in the Supporting Information section), Table 2. As shown in Figure 2B, among $PHPMA_{23}$-*b*-$PDPA_{75}$ nano-objects, a predominant micelle phase is observed, although a small population of polymersomes was found as well (see arrows in Figure S6, Supporting Information section). For $PHPMA_{23}$-*b*-$PDPA_{75}$, DLS analysis indicated that the larger diameter is about 65 nm and relatively broad particle size distributions (PDI = 0.185) (Figure S5, in Supporting Information section); see Table 2. The obtained results could be accepted as evidence of the presence of micelles/polymersomes mixtures. Order−order transitions from micelles to polymersomes states were found for $PHPMA_{23}$-*b*-$PDPA_{100}$ with increasing DP of DPA. The resulting formation of higher order morphologies was favored, and a clear transition from micellar spheres to polymersomes was obtained (Figure 2C). DLS intensity-average diameter is about 123 nm with a relatively narrow particle size distribution (PDI = 0.05), Figure S5 (see the Supporting Information section), Table 2. It might be hypothesized that the incomplete conversion (∼85%) could be another factor allowing the formation of polymersomes. This could occur due to the well-known mechanism of emulsion polymerization[63] because the residual monomer could act as a cosolvent (analogous to dispersion polymerization conditions), swelling the growing particles and allowing particle morphology evolution. However, detailed experiments should be performed in order to clarify this hypothesis.

Furthermore, a comprehensive study using PHPMA-mCTA with DP = 51 and the same DPs for the DPA monomer ($n$ = 50, 75, and 100) was performed. Conversion of the obtained NPs via MWI-PISA polymerization was determined by $^1$H NMR spectroscopy to be quite high (see Table 2). The resulting $PHPMA_{51}$-*b*-$PDPA_n$ diblock copolymers assemblies exhibited a linear increase in the number-average molecular weight ($M_n$) with monomer conversion.

For more accurate copolymer morphology assignments, cryo-TEM (Figure 3) and DLS studies (Figure S7, ESI) were also performed. Typical cryo-TEM images obtained for the PISA formulation $PHPMA_{51}$-*b*-$PDPA_n$ ($n$ = 50, 75, and 100) are shown in Figure 3A, B, and C. The cryo-TEM illustrations for all cases clearly demonstrate the presence of uniform and well-defined spherically assembled micelles. The copolymer assemblies with DP100 was predicted to have vesicle phases because of the weight-fraction ratio of the of hydrophobic and hydrophilic blocks (Table 2, discussed hereafter); however, such morphology was not observed. Of note, the DLS result shows that the hydrodynamic diameter ($D_H$) of all above-mentioned assemblies increases with increasing DP of DPA with a narrow size distribution (see Figure S7, Supporting Information section and Table 2).

The self-assembly process is controlled by the length of the amphiphile blocks as an order parameter in phase transitions:[64,65] changing the order parameter changes the cooperative properties of the self-assembled objects/structures. In this way, it is well known that the resulting morphology of self-assembling structures from block copolymers in solutions is dictated by the relative weight-fraction of hydrophobic and hydrophilic blocks. Hydrophilic weight fractions between 25 and 40% favored the formation of vesicles, between 40 and 50% the formation of cylinders or worms, and higher than 50% the formation of micelles.[66,67] These fractions agreed reasonably well for the assemblies prepared from the lower PHPMA block, $PHPMA_{23}$ (exception for the shorter PDPA) (Table 2). Interestingly, although for the block copolymers manufactured with the longest PHPMA block ($PHPMA_{53}$), the PISA approach allowed the manufacturing of micelles only. In this case, the morphology seems to be driven by the length of the hydrophilic chains rather than by the hydrophilic-to-hydrophobic weight ratio. Indeed, similar results were observed also by others where amphiphilic block copolymers with longer hydrophilic chains favored the formation of micelles and those with shorter hydrophilic chains enabled the manufacturing of polymersomes.[68]

**In Vitro Evaluations of NR-Loaded PISA Formulations.** Aiming at the application for the drug-delivery field, two different pH-responsive PISA formulations (polymersomes (PSs) from $PHPMA_{23}$-*b*-$PDPA_{100}$ and polymeric micelles from $PHPMA_{51}$-*b*-$PDPA_{100}$) were loaded in situ polarity-responsive hydrophobic dye NR as a drug model for the in vitro evaluation of the NP behavior. In the case of PSs, because NR is hydrophobic, the encapsulation of NR is most likely


https://doi.org/10.1021/acsomega.2c04036
ACS Omega 2022, 7, 42711−42722

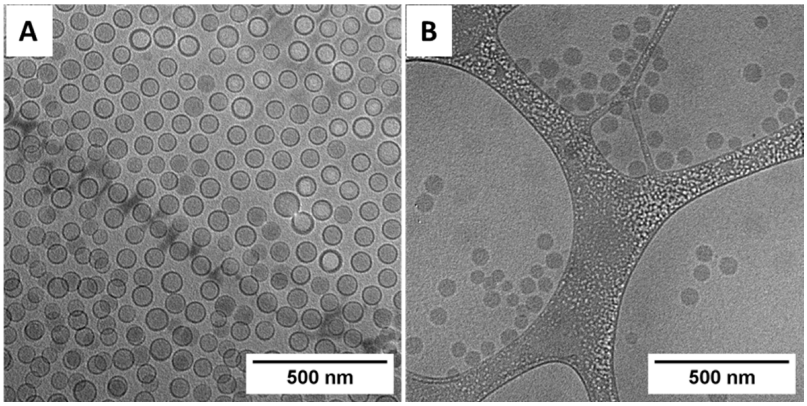


**Figure 4.** Cryo-TEM images of (A) PHPMA$_{23}$-*b*-PDPA$_{100}$-NR- and (B) PHPMA$_{51}$-*b*-PDPA$_{100}$-NR-loaded NPs.

**Table 3. Physicochemical Characteristics of the NR-Loaded PHPMA$_{23}$-*b*-PDPA$_{100}$ and PHPMA$_{51}$-*b*-PDPA$_{100}$ PISA Formulations**

| | $D_H$ (nm) | $R_H$ (nm) | $R_G$ (nm) | $\rho = R_G/R_H$ | $M_w$ ($10^7$ g·mol$^{-1}$) | PDI | $N_{agg}$ |
|---|---|---|---|---|---|---|---|
| PHPMA$_{23}$-*b*-PDPA$_{100}$-NR | 145 | 72.5 | 72 | 0.99 | 2.48 | 0.09 | 1180 |
| PHPMA$_{51}$-*b*-PDPA$_{100}$ NR | 90 | 45 | 51 | 1.13 | 3.96 | 0.12 | 162 |

predicted to be in the membrane of the polymersomes.[69,70] In case of micelles, the NR dye occupies the hydrophobic compartments and it is loaded into the micelle core via hydrophobic interaction with the PDPA segments (Figure 4B).[71−73]

To avoid possible aggregation-induced self-quenching, an optimized theoretical NR loading percentage of 0.20 wt % was carefully selected. This approach demonstrates efficient LC and LE (LE = 34%; LC = 0.24% for PHPMA$_{23}$-*b*-PDPA$_{100}$ and LE = 21%; LC = 0.15% for PHPMA$_{51}$-*b*-PDPA$_{100}$), which was determined by HPLC using a fluorescent detector.

SLS was also performed toward the characterization of the NR-loaded assemblies as a complementary technique to cryo-TEM (see the Supporting Information section for methods). The static and hydrodynamic dimensions of a scattering object are functions of the macromolecular structure. The combination of both may provide qualitative information about its architecture. This can be done using the value of the structure-sensitive parameter ($\rho$), which is defined by the $R_G/R_H$ ratio.[3,49] The obtained values of the structure-sensitive parameter ($\rho = R_G/R_H$) of 1.13 for the micelles and of 0.99 for the polymersomes (Table 3) suggest the prevalence of highly hydrated objects compatible, respectively, to the micellar structure (with a remarkably larger corona due to solvation phenomena)[49,52] and to hollow spheres (PSs).[60,66,67] The SLS measurements also give the $M_w$ of the assemblies than can be used for the determination of the aggregation number ($N_{agg} = M_w$ of self-assemblies obtained by SLS/$M_w$ of unimer accessed by NMR; (see eq S3, in the Supporting Information section)[52,60] toward obtaining information about the assemblies' architecture (Table 3). Higher $N_{agg}$ are expected for vesicular morphologies as obtained for the PSs ($N_{agg}$ = 1180 chains forming one PS)[60,66,67] in comparison with micelles ($N_{agg}$ = 162 chains forming one micelle).[52] Overall the SLS results are in good agreement with the cryo-TEM images, as further evidenced by the morphology of the resulting NPs.

Almost no changes in $D_H$ were observed when NR dye was encapsulated for PHPMA$_{23}$-*b*-PDPA$_{100}$ PSs ($D_H$ = 123 nm NR-free and $D_H$ = 145 nm NR-loaded) with the vesicular morphology retained, whereas for PHPMA$_{51}$-*b*-PDPA$_{100}$ M ($D_H$ = 183 nm NR-free and $D_H$ = 90 nm NR-loaded), despite maintaining the micellar morphology, the $D_H$ was reduced twice. The probable reason for this is that the addition of hydrophobic NR determines the formation of micelles with a more compact core.[63,64] This may be a subject of detailed research in future work. Moreover, in both PISA NR-loaded NPs, no changes in the morphology were observed (see Figure 4), highlighting that the morphological transformations during polymerization in the presence of NR correspond to the transitions observed in the absence of NR.

Moreover, small-angle X-ray scattering measurements (SAXS) was used as a powerful analytical technique to confirm the presence of different morphologies, as shown in Figure 5.

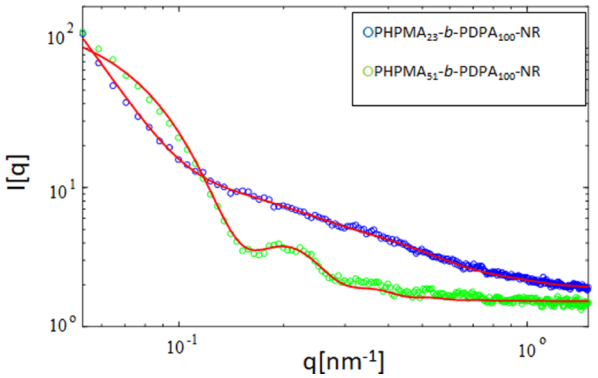


**Figure 5.** SAXS patterns for (blue circle) PHPMA$_{23}$-*b*-PDPA100-NR-polymersomes and (green circle) PHPMA$_{51}$-*b*-PDPA$_{100}$-NR core−shell micelles along with the corresponding curve fittings (solid lines).

SAXS data were recorded for PHPMA$_{23}$-*b*-PDPA$_{100}$-NR and PHPMA$_{51}$-*b*-PDPA$_{100}$-NR nano-objects and could be successfully fitted using a core−shell sphere model with log-norm distribution of the outer size and the resulting scattering patterns modeled using spherical micelles[74] and vesicles[75] plus the Gaussian polymer chains model as a background.[76]

$$I(q) \sim K^2\,(q, R, \Delta\eta) + \text{background} \quad (3)$$



https://doi.org/10.1021/acsomega.2c04036
ACS Omega 2022, 7, 42711−42722

where

$$K(q, R, \Delta\eta) = \frac{4}{3}\pi R3\ \Delta\eta 3\frac{\sin(qR) - qR\cos(qR)}{(qR)3} \quad (4)$$

is the scattering from spherical NPs of radius $R$, $\Delta\eta$ is the difference between the scattering length density of the polymer and the solvent. The $q^{-2}$ dependence at the low-$q$ range is expected for the polymeric vesicles, and the SAXS profiles portrayed in Figure 5 (open blue circles) could only be decently fitted by using the form factor of the bilayered vesicles. This is at the edge of the lowest q-region we are able to reach. The radius of PSs for the hydrophilic PHPMA shell is $R1$ = 85.1 nm and the radius of the hydrophopic PDPA layer is $R2$ = 12.6 nm with a scattering length density difference between shell and matrix $\Delta\eta$ = 0.02, as well as scattering shell density difference between layer and matrix relative to the shell contrast $\mu$ = 0.99. On the other hand, the near-$q^0$ dependence of the SAXS profiles evidenced in Figure 5 (open green circles) points out the formation of core−shell spherical aggregates for the $PHPMA_{51}$-*b*-PDPA100-NR micelles. The values found for NR core−shell micelles were $R$ = 17.8 nm and $R_g$shell = 17.0 nm, resulting in a total particle radius ($R + R_g$shell) of 34.8 nm, which is slightly smaller than the $R_g$ determined through SLS ($R_g$ = 51 nm). The scattering length density difference between the shell and matrix is $\Delta\eta = 4 \times 10^{-4}$, and the scattering shell density difference between the core and matrix relative to the shell contrast is $\mu$ = 0.29. Overall, these data and the respective curve fittings confirm the self-assembly of the diblock copolymers $PHPMA_{23}$-*b*-$PDPA_{100}$-NR into polymersomes and $PHPMA_{51}$-*b*-$PDPA_{100}$-NR into micelles.

Next, the release of NR was studied under simulated physiological conditions at pH ∼ 7.4 in PBS and acidic acetate buffer at pH ∼ 4. The release profiles are given in Figure 6.

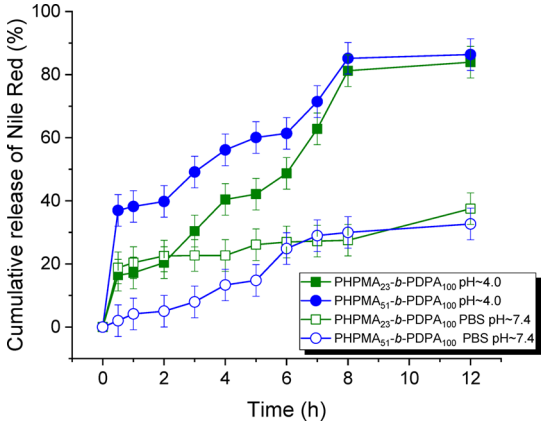


**Figure 6.** NR cumulative release from $PHPMA_{23}$-*b*-$PDPA_{100}$ vesicles and $PHPMA_{51}$-*b*-$PDPA_{100}$ micelles at pH ∼ 4 and pH ∼ 7.4.

The mechanism for drug release in pH response systems is well known and is as follows: at pH values above 6.2−6.3, the NR-loaded NPs produced a strong fluorescence intensity owing to the hydrophobic microenvironment inside the micelle core. At pH values below 6.0, the PDPA core dissociated, and the NR payload was released into the aqueous phase, thus causing dramatic quenching of the fluorescent signal.[73,77]

The release profiles of $PHPMA_{23}$-*b*-$PDPA_{100}$-NR-loaded vesicles demonstrated that at acidic pH ∼ 4 after 4 h, 40% was released and 84% after 12 h (filled green squares). Likewise, in the case of simulated physiological pH ∼ 7.4, the release was 22% in 4 h and 37% after 12 h (open green squares). The release profiles in the case of $PHPMA_{51}$-*b*-$PDPA_{100}$-NR-loaded micelles showed that more than 50% of the loaded dye was released within 4 h at pH ∼ 4 and 86% after 12 h (filled blue circles). Under neutral physiological conditions, PBS pH ∼ 7.4 at 4 h release reached 13 and 32% after 12 h (open blue circles). The obtained results demonstrate that PSs at pH > p$K_a$ which points out to a higher ability to efficiently deliver the payload to the pH-specific site without higher amounts being released at pH 7.4.[61,62] These results are compatible with the release of payloads from systems based on the PDPA core observed by us[51,61,77] and others[78,79] In contrast, at pH < p$K_a$, because of protonation of the PDPA block, the NPs undergo physical disassembly that lead to quick release of loaded NR.[61] It has already been reported by others that PSs show higher stability and slow release in buffered conditions than micelles.[80,81] It is important to highlight that the observed retardation of the NR release after an initial fast release at pH ∼ 4.0 is explained because the pH-induced disassembly at pHs lower than the pKa of the PDPA block leads to the presence of free chains that can reorganize in order to avoid as much as possible the contact with the polar solvent, water. These chains as unimers entrapped again the NR used and are most likely responsible for the retardation of the release even at pHs below the p$K_a$ of the PDPA block. This has been studied previously by fluorescence energy transfer experiments (FRET) using the pair dyes cyanine 3- and cyanine 5 covalently bound to the PHPMA-*b*-PDPA block forming Cy3-Cy5-polymersomes.[61] However, it is important to be mentioned that this reorganization seems not to interfere in the in vivo effect of similar PSs of PHPMA-*b*-PDPA that greatly enhanced the therapeutic efficacy with effective inhibition of EL4 lymphoma tumors in a mouse model with a 100% survival rate,[77] highlighting the potential of such block copolymers in the drug-delivery field.

**pH-Responsive Behavior of NPs Prepared by PISA.** Because the PDPA block is pH-responsive (p$K_a$ ∼ 6.2−6.3),[51] that is, it is deprotonated and hydrophobic under neutral conditions and changes into protonated and hydrophilic state in acidic solution,[55] an additional study on the stimuli-responsive behavior of the NPs $PHPMA_{23}$-*b*-$PDPA_{100}$ (PSs) and $PHPMA_{51}$-*b*-$PDPA_{100}$ (M) was performed. The spherical NPs were dispersed into neutral aqueous solution with a final concentration of approximately 1 mg·mL$^{-1}$, and this behavior was monitored by DLS over time. The NPs were observed to be stable in PBS pH ∼ 7.4 at 37 °C, which is a consequence of the p$K_a$ of PDPA (p$K_a$ ∼ 6.3).[51] In contrast, at pH ∼ 4.0, the NPs quickly disassembled, while the block copolymer formulations behaved as protonated single dissolved polymer chains in an acidic medium. Because the light scattering intensity is proportional to the concentration of particles, their disassembly leads to a significant reduction in light scattering.[61] The scattering intensity $I_{sc}$ at pH ∼ 4.0 decreases by almost 100% compared to $I_{sc}$ in PBS over 5 min for micelles prepared from $PHPMA_{51}$-*b*-$PDPA_{100}$ (open blue circles) and in less than a minute for polymersomes of $PHPMA_{23}$-*b*-$PDPA_{100}$ (open red circles) (see Figure 7). Interestingly, this higher stability under buffered simulated physiological conditions (pH ∼ 7.4) and ultrafast disassembly at acidic pH is desirable and a straightforward strategy for cargo delivery, for example, chemotherapeutics to tumor sites with high efficiency.


https://doi.org/10.1021/acsomega.2c04036
ACS Omega 2022, 7, 42711−42722

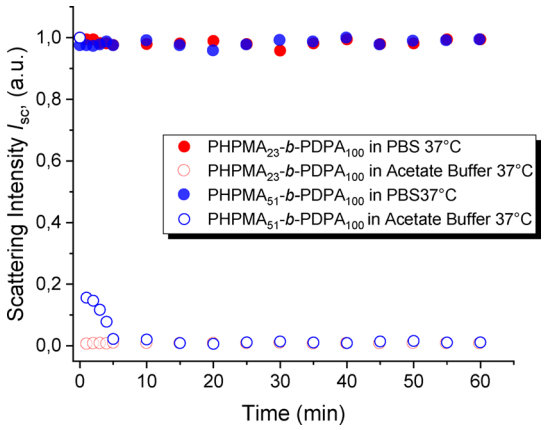


**Figure 7.** pH-responsive behavior studied by changes in light scattering intensity ($I_{sc}$) after incubation of micelles and vesicles in PBS pH ∼ 7.4 and pH ∼ 4.0 at 37 °C.

## CONCLUSIONS

Herein, we have highlighted the first evaluation of the effect of microwave irradiation-mediated conditions on pH-responsive PHPMA$_m$-*b*-PDPA$_n$ in situ soft matter nanoparticle formation in purely aqueous solution via PISA. We have demonstrated that the MWI-PISA aqueous RAFT polymerization proceeded with reasonably good control, achieving elevated conversions (∼85%) within a short period of time (4 h). The copolymer morphology results were found to be limited to spheres [micelles (M) and polymersomes (PSs)] only, and no micelle-worm-polymerosome transition was observed, which is probably due to the reaction conditions we chose. Of note, the morphology of nanoassemblies synthesized by PISA can be easily tuned from micelles to polymersomes by changing the DP of the hydrophilic and/or hydrophobic block.

Furthermore, NR-loaded pH-responsive polymeric spheres (M + PSs) using the block copolymer PHPMA$_m$-*b*-PDPA$_{100}$ as the building unit are reported. Spherical nanoparticles can stably encapsulate hydrophobic compounds inside their hydrophobic PDPA cores (M) or walls (PSs) *via* hydrophobic interactions. It was found that the polymersomes of PHPMA$_{23}$-*b*-PDPA$_{100}$ have increased the encapsulation efficiency, better stability at physiological pH, and faster release at acidic pH compared to formulation PHPMA$_{51}$-*b*-PDPA$_{100}$ with the micellar morphology. The capability of fine-tuning the morphology from micelles to polymersomes herein with drug encapsulation may attract considerable attention in the drug-delivery field.

## ASSOCIATED CONTENT

### Supporting Information

The Supporting Information is available free of charge at https://pubs.acs.org/doi/10.1021/acsomega.2c04036.

Instruments and analyses; synthesis of monomer; 1H NMR spectra results; SEC analysis results; dynamic light scattering particle size distributions; and cryo-TEM image (PDF)

## AUTHOR INFORMATION

### Corresponding Authors

**Svetlana Lukáš Petrova** − *Institute of Macromolecular Chemistry v.v.i., Academy of Sciences of the Czech Republic, 162 06 Prague, Czech Republic*; orcid.org/0000-0001-7364-4737; Email: petrova@imc.cas.cz

**Vladimir Sincari** − *Institute of Macromolecular Chemistry v.v.i., Academy of Sciences of the Czech Republic, 162 06 Prague, Czech Republic*; orcid.org/0000-0002-7379-066X; Email: sincari@imc.cas.cz

### Authors

**Rafał Konefał** − *Institute of Macromolecular Chemistry v.v.i., Academy of Sciences of the Czech Republic, 162 06 Prague, Czech Republic*

**Ewa Pavlova** − *Institute of Macromolecular Chemistry v.v.i., Academy of Sciences of the Czech Republic, 162 06 Prague, Czech Republic*

**Martin Hrubý** − *Institute of Macromolecular Chemistry v.v.i., Academy of Sciences of the Czech Republic, 162 06 Prague, Czech Republic*; orcid.org/0000-0002-5075-261X

**Václav Pokorný** − *Institute of Macromolecular Chemistry v.v.i., Academy of Sciences of the Czech Republic, 162 06 Prague, Czech Republic*; orcid.org/0000-0003-4145-7982

**Eliézer Jäger** − *Institute of Macromolecular Chemistry v.v.i., Academy of Sciences of the Czech Republic, 162 06 Prague, Czech Republic*; orcid.org/0000-0001-9939-2355

Complete contact information is available at: https://pubs.acs.org/10.1021/acsomega.2c04036

### Author Contributions

S.L.P. performed the synthesis and wrote the manuscript. V.S. conceived the idea for the synthesis of PHPMA-*b*-PDPA diblock copolymer via PISA self-assembly, performed the synthesis, and wrote the manuscript. E.J. performed DLS experiments, analyzed DLS data, wrote the manuscript, and gave the financial support. R.K. performed NMR experiments. E.P. performed cryo-TEM experiments. V.P. performed X-ray experiments and M.H. analyzed the data and gave the financial support.

### Funding

This work was supported by Czech Science Foundation Grant # 20-15077Y and 21-01090S and by the Ministry of Education, Youth and Sports of the Czech Republic (Grant # EATRIS-CZ LM2018133 ERIC).

### Notes

The authors declare no competing financial interest.

## ACKNOWLEDGMENTS

E.J. is thanked for the Czech Science Foundation (Grant # 20-15077Y) and M.H acknowledges the Czech Science Foundation (Grant # 21-01090S) and the Ministry of Education, Youth and Sports of the Czech Republic (Grant # EATRIS-CZ LM2018133 ERIC).

## REFERENCES

(1) Canning, S. L.; Smith, G. N.; Armes, S. P. A Critical Appraisal of RAFT-Mediated Polymerization-Induced Self-Assembly. *Macromolecules* **2016**, *49*, 1985−2001.

(2) Mai, Y.; Eisenberg, A. Self-Assembly of Block Copolymers. *Chem. Soc. Rev.* **2012**, *41*, 5969.

(3) Rodriguezhernandez, J.; Checot, F.; Gnanou, Y.; Lecommandoux, S. Toward 'Smart' Nano-Objects by Self-Assembly of Block Copolymers in Solution. *Prog. Polym. Sci.* **2005**, *30*, 691−724.

(4) Zhang, L.; Eisenberg, A. Multiple Morphologies of "Crew-Cut" Aggregates of Polystyrene-b-Poly(Acrylic Acid) Block Copolymers. *Science* **1995**, *268*, 1728−1731.
(5) Jia, L.; Zhao, G.; Shi, W.; Coombs, N.; Gourevich, I.; Walker, G. C.; Guerin, G.; Manners, I.; Winnik, M. A. A Design Strategy for the Hierarchical Fabrication of Colloidal Hybrid Mesostructures. *Nat. Commun.* **2014**, *5*, 3882.
(6) Reynhout, I. C.; Cornelissen, J. J. L. M.; Nolte, R. J. M. Synthesis of Polymer-Biohybrids: From Small to Giant Surfactants. *Acc. Chem. Res.* **2009**, *42*, 681.
(7) Tan, J.; Bai, Y.; Zhang, X.; Zhang, L. Room Temperature Synthesis of Poly(Poly(Ethylene Glycol) Methyl Ether Methacrylate)-Based Diblock Copolymer Nano-Objects via Photoinitiated Polymerization-Induced Self-Assembly (Photo-PISA). *Polym. Chem.* **2016**, *7*, 2372−2380.
(8) Zhang, J.; Wang, L.-Q.; Wang, H.; Tu, K. Micellization Phenomena of Amphiphilic Block Copolymers Based on Methoxy Poly(Ethylene Glycol) and Either Crystalline or Amorphous Poly(Caprolactone-b-Lactide). *Biomacromolecules* **2006**, *7*, 2492−2500.
(9) Charleux, B.; Delaittre, G.; Rieger, J.; D'Agosto, F. Polymerization-Induced Self-Assembly: From Soluble Macromolecules to Block Copolymer Nano-Objects in One Step. *Macromolecules* **2012**, *45*, 6753−6765.
(10) Li, S.; Han, G.; Zhang, W. Cross-Linking Approaches for Block Copolymer Nano-Assemblies via RAFT-Mediated Polymerization-Induced Self-Assembly. *Polym. Chem.* **2020**, *11*, 4681−4692.
(11) Yeow, J.; Boyer, C. Photoinitiated Polymerization-Induced Self-Assembly (Photo-PISA): New Insights and Opportunities. *Adv. Sci.* **2017**, *4*, No. 1700137.
(12) Biais, P.; Colombani, O.; Bouteiller, L.; Stoffelbach, F.; Rieger, J. Unravelling the Formation of BAB Block Copolymer Assemblies during PISA in Water. *Polym. Chem.* **2020**, *11*, 4568−4578.
(13) Gonzato, C.; Semsarilar, M.; Jones, E. R.; Li, F.; Krooshof, G. J. P.; Wyman, P.; Mykhaylyk, O. O.; Tuinier, R.; Armes, S. P. Rational Synthesis of Low-Polydispersity Block Copolymer Vesicles in Concentrated Solution via Polymerization-Induced Self-Assembly. *J. Am. Chem. Soc.* **2014**, *136*, 11100−11106.
(14) Warren, N. J.; Armes, S. P. Polymerization-Induced Self-Assembly of Block Copolymer Nano-Objects via RAFT Aqueous Dispersion Polymerization. *J. Am. Chem. Soc.* **2014**, *136*, 10174−10185.
(15) Blackman, L. D.; Doncom, K. E. B.; Gibson, M. I.; O'Reilly, R. K. Comparison of Photo- and Thermally Initiated Polymerization-Induced Self-Assembly: A Lack of End Group Fidelity Drives the Formation of Higher Order Morphologies. *Polym. Chem.* **2017**, *8*, 2860−2871.
(16) Fielding, L. A.; Derry, M. J.; Ladmiral, V.; Rosselgong, J.; Rodrigues, A. M.; Ratcliffe, L. P. D.; Sugihara, S.; Armes, S. P. RAFT Dispersion Polymerization in Non-Polar Solvents: Facile Production of Block Copolymer Spheres, Worms and Vesicles in n-Alkanes. *Chem. Sci.* **2013**, *4*, 2081.
(17) Khan, H.; Cao, M.; Duan, W.; Ying, T.; Zhang, W. Synthesis of Diblock Copolymer Nano-Assemblies: Comparison between PISA and Micellization. *Polymer* **2018**, *150*, 204−213.
(18) György, C.; Hunter, S. J.; Girou, C.; Derry, M. J.; Armes, S. P. Synthesis of Poly(Stearyl Methacrylate)-Poly(2-Hydroxypropyl Methacrylate) Diblock Copolymer Nanoparticles via RAFT Dispersion Polymerization of 2-Hydroxypropyl Methacrylate in Mineral Oil. *Polym. Chem.* **2020**, *11*, 4579−4590.
(19) Zeng, M.; Cao, X.; Xu, H.; Gan, W.; Smith, B. D.; Gao, H.; Yuan, J. Synthesis and Direct Assembly of Linear−Dendritic Copolymers via CuAAC Click Polymerization-Induced Self-Assembly (CPISA). *Polym. Chem.* **2020**, *11*, 936−943.
(20) Sarkar, J.; Xiao, L.; Jackson, A. W.; van Herk, A. M.; Goto, A. Synthesis of Transition-Metal-Free and Sulfur-Free Nanoparticles and Nanocapsules via Reversible Complexation Mediated Polymerization (RCMP) and Polymerization Induced Self-Assembly (PISA). *Polym. Chem.* **2018**, *9*, 4900−4907.
(21) Zhang, Y.; Han, G.; Cao, M.; Guo, T.; Zhang, W. Influence of Solvophilic Homopolymers on RAFT Polymerization-Induced Self-Assembly. *Macromolecules* **2018**, *51*, 4397−4406.
(22) Cornel, E. J.; Jiang, J.; Chen, S.; Du, J. Principles and Characteristics of Polymerization-Induced Self-Assembly with Various Polymerization Techniques. *CCS Chem.* **2021**, *3*, 2104−2125.
(23) Moad, G.; Rizzardo, E.; Thang, S. H. Toward Living Radical Polymerization. *Acc. Chem. Res.* **2008**, *41*, 1133−1142.
(24) Perrier, S. 50th Anniversary Perspective : RAFT Polymerization—A User Guide. *Macromolecules* **2017**, *50*, 7433−7447.
(25) Chong, Y. K.; Krstina, J.; Le, T. P. T.; Moad, G.; Postma, A.; Rizzardo, E.; Thang, S. H. Thiocarbonylthio Compounds [SC(Ph)S−R] in Free Radical Polymerization with Reversible Addition-Fragmentation Chain Transfer (RAFT Polymerization). Role of the Free-Radical Leaving Group (R). *Macromolecules* **2003**, *36*, 2256−2272.
(26) Cai, W.; Wan, W.; Hong, C.; Huang, C.; Pan, C. Morphology Transitions in RAFT Polymerization. *Soft Matter* **2010**, *6*, 5554.
(27) Semsarilar, M.; Jones, E. R.; Armes, S. P. Comparison of Pseudo-Living Character of RAFT Polymerizations Conducted under Homogeneous and Heterogeneous Conditions. *Polym. Chem.* **2014**, *5*, 195−203.
(28) Fielding, L. A.; Lane, J. A.; Derry, M. J.; Mykhaylyk, O. O.; Armes, S. P. Thermo-Responsive Diblock Copolymer Worm Gels in Non-Polar Solvents. *J. Am. Chem. Soc.* **2014**, *136*, 5790−5798.
(29) Blanazs, A.; Ryan, A. J.; Armes, S. P. Predictive Phase Diagrams for RAFT Aqueous Dispersion Polymerization: Effect of Block Copolymer Composition, Molecular Weight, and Copolymer Concentration. *Macromolecules* **2012**, *45*, 5099−5107.
(30) Sugihara, S.; Armes, S. P.; Blanazs, A.; Lewis, A. L. Non-Spherical Morphologies from Cross-Linked Biomimetic Diblock Copolymers Using RAFT Aqueous Dispersion Polymerization. *Soft Matter* **2011**, *7*, 10787.
(31) Cunningham, V. J.; Alswieleh, A. M.; Thompson, K. L.; Williams, M.; Leggett, G. J.; Armes, S. P.; Musa, O. M. Poly(Glycerol Monomethacrylate)−Poly(Benzyl Methacrylate) Diblock Copolymer Nanoparticles via RAFT Emulsion Polymerization: Synthesis, Characterization, and Interfacial Activity. *Macromolecules* **2014**, *47*, 5613−5623.
(32) Rieger, J.; Stoffelbach, F.; Bui, C.; Alaimo, D.; Jérôme, C.; Charleux, B. Amphiphilic Poly(Ethylene Oxide) Macromolecular RAFT Agent as a Stabilizer and Control Agent in Ab Initio Batch Emulsion Polymerization. *Macromolecules* **2008**, *41*, 4065−4068.
(33) Ferguson, C. J.; Hughes, R. J.; Pham, B. T. T.; Hawkett, B. S.; Gilbert, R. G.; Serelis, A. K.; Such, C. H. Effective Ab Initio Emulsion Polymerization under RAFT Control. *Macromolecules* **2002**, *35*, 9243−9245.
(34) Yeole, N.; Hundiwale, D.; Jana, T. Synthesis of Core−Shell Polystyrene Nanoparticles by Surfactant Free Emulsion Polymerization Using Macro-RAFT Agent. *J. Colloid Interface Sci.* **2011**, *354*, 506−510.
(35) Yeole, N.; Kutcherlapati, S. N. R.; Jana, T. Tunable Core−Shell Nanoparticles: Macro-RAFT Mediated One Pot Emulsion Polymerization. *RSC Adv.* **2013**, *4*, 2382−2388.
(36) Neal, T. J.; Penfold, N. J. W.; Armes, S. P. Reverse Sequence Polymerization-Induced Self-Assembly in Aqueous Media. *Angew. Chem., Int. Ed.* **2022**, *61*, No. e202207376.
(37) Chan, D. H. H.; Cockram, A. A.; Gibson, R. R.; Kynaston, E. L.; Lindsay, C.; Taylor, P.; Armes, S. P. RAFT Aqueous Emulsion Polymerization of Methyl Methacrylate: Observation of Unexpected Constraints When Employing a Non-Ionic Steric Stabilizer Block. *Polym. Chem.* **2021**, *12*, 5760−5769.
(38) North, S. M.; Armes, S. P. One-Pot Synthesis and Aqueous Solution Properties of PH-Responsive Schizophrenic Diblock Copolymer Nanoparticles Prepared via RAFT Aqueous Dispersion Polymerization. *Polym. Chem.* **2021**, *12*, 5842−5850.
(39) Hunter, S. J.; Lovett, J. R.; Mykhaylyk, O. O.; Jones, E. R.; Armes, S. P. Synthesis of Diblock Copolymer Spheres, Worms and


https://doi.org/10.1021/acsomega.2c04036
*ACS Omega* 2022, 7, 42711−42722

Vesicles via RAFT Aqueous Emulsion Polymerization of Hydroxybutyl Methacrylate. *Polym. Chem.* **2021**, *12*, 3629−3639.
(40) Semsarilar, M.; Ladmiral, V.; Blanazs, A.; Armes, S. P. Anionic Polyelectrolyte-Stabilized Nanoparticles via RAFT Aqueous Dispersion Polymerization. *Langmuir* **2012**, *28*, 914−922.
(41) He, W.-D.; Sun, X.-L.; Wan, W.-M.; Pan, C.-Y. Multiple Morphologies of PAA-b-PSt Assemblies throughout RAFT Dispersion Polymerization of Styrene with PAA Macro-CTA. *Macromolecules* **2011**, *44*, 3358−3365.
(42) Wan, W.-M.; Sun, X.-L.; Pan, C.-Y. Morphology Transition in RAFT Polymerization for Formation of Vesicular Morphologies in One Pot. *Macromolecules* **2009**, *42*, 4950−4952.
(43) Pei, Y.; Lowe, A. B. Polymerization-Induced Self-Assembly: Ethanolic RAFT Dispersion Polymerization of 2-Phenylethyl Methacrylate. *Polym. Chem.* **2014**, *5*, 2342−2351.
(44) Zhang, X.; Boissé, S.; Zhang, W.; Beaunier, P.; D'Agosto, F.; Rieger, J.; Charleux, B. Well-Defined Amphiphilic Block Copolymers and Nano-Objects Formed in Situ via RAFT-Mediated Aqueous Emulsion Polymerization. *Macromolecules* **2011**, *44*, 4149−4158.
(45) Cockram, A. A.; Neal, T. J.; Derry, M. J.; Mykhaylyk, O. O.; Williams, N. S. J.; Murray, M. W.; Emmett, S. N.; Armes, S. P. Effect of Monomer Solubility on the Evolution of Copolymer Morphology during Polymerization-Induced Self-Assembly in Aqueous Solution. *Macromolecules* **2017**, *50*, 796−802.
(46) Byard, S. J.; O'Brien, C. T.; Derry, M. J.; Williams, M.; Mykhaylyk, O. O.; Blanazs, A.; Armes, S. P. Unique Aqueous Self-Assembly Behavior of a Thermoresponsive Diblock Copolymer. *Chem. Sci.* **2020**, *11*, 396−402.
(47) Blanazs, A.; Madsen, J.; Battaglia, G.; Ryan, A. J.; Armes, S. P. Mechanistic Insights for Block Copolymer Morphologies: How Do Worms Form Vesicles? *J. Am. Chem. Soc.* **2011**, *133*, 16581−16587.
(48) Warren, N. J.; Mykhaylyk, O. O.; Mahmood, D.; Ryan, A. J.; Armes, S. P. RAFT Aqueous Dispersion Polymerization Yields Poly(Ethylene Glycol)-Based Diblock Copolymer Nano-Objects with Predictable Single Phase Morphologies. *J. Am. Chem. Soc.* **2014**, *136*, 1023−1033.
(49) Semsarilar, M.; Ladmiral, V.; Blanazs, A.; Armes, S. P. Cationic Polyelectrolyte-Stabilized Nanoparticles via RAFT Aqueous Dispersion Polymerization. *Langmuir* **2013**, *29*, 7416−7424.
(50) Ladmiral, V.; Charlot, A.; Semsarilar, M.; Armes, S. P. Synthesis and Characterization of Poly(Amino Acid Methacrylate)-Stabilized Diblock Copolymer Nano-Objects. *Polym. Chem.* **2015**, *6*, 1805−1816.
(51) Jäger, E.; Jäger, A.; Etrych, T.; Giacomelli, F. C.; Chytil, P.; Jigounov, A.; Putaux, J.-L.; Říhová, B.; Ulbrich, K.; Štěpánek, P. Self-Assembly of Biodegradable Copolyester and Reactive HPMA-Based Polymers into Nanoparticles as an Alternative Stealth Drug Delivery System. *Soft Matter* **2012**, *8*, 9563.
(52) Duncan, R.; Vicent, M. J. Do HPMA Copolymer Conjugates Have a Future as Clinically Useful Nanomedicines? A Critical Overview of Current Status and Future Opportunities☆. *Adv. Drug Delivery Rev.* **2010**, *62*, 272−282.
(53) Talelli, M.; Rijcken, C. J. F.; van Nostrum, C. F.; Storm, G.; Hennink, W. E. Micelles Based on HPMA Copolymers☆. *Adv. Drug Delivery Rev.* **2010**, *62*, 231−239.
(54) Kopeček, J.; Kopečková, P. HPMA Copolymers: Origins, Early Developments, Present, and Future☆. *Adv. Drug Delivery Rev.* **2010**, *62*, 122−149.
(55) Giacomelli, F. C.; Stepánek, P.; Giacomelli, C.; Schmidt, V.; Jäger, E.; Jäger, A.; Ulbrich, K. PH-Triggered Block Copolymer Micelles Based on a PH-Responsive PDPA (Poly[2-(Diisopropylamino)Ethyl Methacrylate]) Inner Core and a PEO (Poly(Ethylene Oxide)) Outer Shell as a Potential Tool for the Cancer Therapy. *Soft Matter* **2011**, *7*, 9316.
(56) Bütün, V.; Armes, S.; Billingham, N. Synthesis and Aqueous Solution Properties of Near-Monodisperse Tertiary Amine Methacrylate Homopolymers and Diblock Copolymers. *Polymer* **2001**, *42*, 5993−6008.
(57) Garrett, E. T.; Pei, Y.; Lowe, A. B. Microwave-Assisted Synthesis of Block Copolymer Nanoparticles via RAFT with Polymerization-Induced Self-Assembly in Methanol. *Polym. Chem.* **2016**, *7*, 297−301.
(58) Sincari, V.; Petrova, S. L.; Konefał, R.; Hruby, M.; Jäger, E. Microwave-Assisted RAFT Polymerization of N-(2-Hydroxypropyl) Methacrylamide and Its Relevant Copolymers. *React. Funct. Polym.* **2021**, *162*, No. 104875.
(59) Ulbrich, K.; Šubr, V.; Strohalm, J.; Plocová, D.; Jelínková, M.; Říhová, B. Polymeric Drugs Based on Conjugates of Synthetic and Natural Macromolecules. *J. Controlled Release* **2000**, *64*, 63−79.
(60) Danial, M.; Telwatte, S.; Tyssen, D.; Cosson, S.; Tachedjian, G.; Moad, G.; Postma, A. Combination Anti-HIV Therapy via Tandem Release of Prodrugs from Macromolecular Carriers. *Polym. Chem.* **2016**, *7*, 7477−7487.
(61) Albuquerque, L. J. C.; Sincari, V.; Jäger, A.; Konefał, R.; Pánek, J.; Černoch, P.; Pavlova, E.; Štěpánek, P.; Giacomelli, F. C.; Jäger, E. Microfluidic-Assisted Engineering of Quasi-Monodisperse PH-Responsive Polymersomes toward Advanced Platforms for the Intracellular Delivery of Hydrophilic Therapeutics. *Langmuir* **2019**, *35*, 8363−8372.
(62) Jones, E. R.; Semsarilar, M.; Wyman, P.; Boerakker, M.; Armes, S. P. Addition of Water to an Alcoholic RAFT PISA Formulation Leads to Faster Kinetics but Limits the Evolution of Copolymer Morphology. *Polym. Chem.* **2016**, *7*, 851−859.
(63) Lovell, P. A.; Schork, F. J. Fundamentals of Emulsion Polymerization. *Biomacromolecules* **2020**, *21*, 4396−4441.
(64) Desai, R. C.; Kapral, R.Propagating Chemical Fronts. In *Dynamics of Self-Organized and Self-Assembled Structures*; Cambridge University Press, 2009; pp 157−163.
(65) Podgornik, R. Principles of Condensed Matter Physics. *J. Stat. Phys.* **1996**, *83*, 1263−1265.
(66) Blanazs, A.; Armes, S. P.; Ryan, A. J. Self-Assembled Block Copolymer Aggregates: From Micelles to Vesicles and Their Biological Applications. *Macromol. Rapid Commun.* **2009**, *30*, 267−277.
(67) Antonietti, M.; Förster, S. Vesicles and Liposomes: A Self-Assembly Principle Beyond Lipids. *Adv. Mater.* **2003**, *15*, 1323−1333.
(68) Černoch, P.; Jager, A.; Černochová, Z.; Sincari, V.; Albuquerque, L. J. C.; Konefal, R.; Pavlova, E.; Giacomelli, F. C.; Jager, E. Engineering of PH-Triggered Nanoplatforms Based on Novel Poly(2-Methyl-2-Oxazoline)- b -Poly[2-(Diisopropylamino)Ethyl Methacrylate] Diblock Copolymers with Tunable Morphologies for Biomedical Applications. *Polym. Chem.* **2021**, *12*, 2868−2880.
(69) Liao, J.; Li, W.; Peng, J.; Yang, Q.; Li, H.; Wei, Y.; Zhang, X.; Qian, Z. Combined Cancer Photothermal-Chemotherapy Based on Doxorubicin/Gold Nanorod-Loaded Polymersomes. *Theranostics* **2015**, *5*, 345−356.
(70) Wu, M.; Zhu, Y.; Jiang, W. Release Behavior of Polymeric Vesicles in Solution Controlled by External Electrostatic Field. *ACS Macro Lett.* **2016**, *5*, 1212−1216.
(71) Greenspan, P.; Mayer, E. P.; Fowler, S. D. Nile Red: A Selective Fluorescent Stain for Intracellular Lipid Droplets. *J. Cell Biol.* **1985**, *100*, 965−973.
(72) Diaz, G.; Melis, M.; Batetta, B.; Angius, F.; Falchi, A. M. Hydrophobic Characterization of Intracellular Lipids in Situ by Nile Red Red/Yellow Emission Ratio. *Micron* **2008**, *39*, 819−824.
(73) Yu, H.; Xu, Z.; Wang, D.; Chen, X.; Zhang, Z.; Yin, Q.; Li, Y. Intracellular PH-Activated PEG-b-PDPA Wormlike Micelles for Hydrophobic Drug Delivery. *Polym. Chem.* **2013**, *4*, 5052.
(74) Pedersen, J. S. Form Factors of Block Copolymer Micelles with Spherical, Ellipsoidal and Cylindrical Cores. *J. Appl. Crystallogr.* **2000**, *33*, 637−640.
(75) Bang, J.; Jain, S.; Li, Z.; Lodge, T. P.; Pedersen, J. S.; Kesselman, E.; Talmon, Y. Sphere, Cylinder, and Vesicle Nanoaggregates in Poly(Styrene-b-Isoprene) Diblock Copolymer Solutions. *Macromolecules* **2006**, *39*, 1199−1208.
(76) Akpinar, B.; Fielding, L. A.; Cunningham, V. J.; Ning, Y.; Mykhaylyk, O. O.; Fowler, P. W.; Armes, S. P. Determining the


https://doi.org/10.1021/acsomega.2c04036
*ACS Omega* 2022, 7, 42711−42722

Effective Density and Stabilizer Layer Thickness of Sterically Stabilized Nanoparticles. *Macromolecules* **2016**, *49*, 5160−5171.
(77) Albuquerque, L. J. C.; Sincari, V.; Jäger, A.; Kucka, J.; Humajova, J.; Pankrac, J.; Paral, P.; Heizer, T.; Janouškova, O.; Davidovich, I.; Talmon, Y.; Pouckova, P.; Štěpánek, P.; Sefc, L.; Hruby, M.; Giacomelli, F. C.; Jäger, E. PH-Responsive Polymersome-Mediated Delivery of Doxorubicin into Tumor Sites Enhances the Therapeutic Efficacy and Reduces Cardiotoxic Effects. *J. Controlled Release* **2021**, *332*, 529−538.
(78) Giacomelli, C.; Le Men, L.; Borsali, R.; Lai-Kee-Him, J.; Brisson, A.; Armes, S. P.; Lewis, A. L. Phosphorylcholine-Based PH-Responsive Diblock Copolymer Micelles as Drug Delivery Vehicles: Light Scattering, Electron Microscopy, and Fluorescence Experiments. *Biomacromolecules* **2006**, *7*, 817−828.
(79) Sun, J.; Wang, Z.; Cao, A.; Sheng, R. Synthesis of Crosslinkable Diblock Terpolymers PDPA-b-P(NMS-co-OEG) and Preparation of Shell-Crosslinked PH/Redox-Dual Responsive Micelles as Smart Nanomaterials. *RSC Adv.* **2019**, *9*, 34535−34546.
(80) Alibolandi, M.; Ramezani, M.; Abnous, K.; Sadeghi, F.; Hadizadeh, F. Comparative Evaluation of Polymersome versus Micelle Structures as Vehicles for the Controlled Release of Drugs. *J. Nanopart. Res.* **2015**, *17*, 76.
(81) Lu, Y.; Zhang, E.; Yang, J.; Cao, Z. Strategies to Improve Micelle Stability for Drug Delivery. *Nano Res.* **2018**, *11*, 4985−4998.



https://doi.org/10.1021/acsomega.2c04036
*ACS Omega* 2022, 7, 42711−42722